

Electrodeposition of Sb onto the low-index planes of Cu in aqueous chloride solutions: studies by LEED, AES and electrochemistry

Lindell C. Ward and John L. Stickney*

Department of Chemistry, University of Georgia, Athens, GA 30602-2556, USA

Received 2nd March 2001, Accepted 25th April 2001

First published as an Advance Article on the web 30th May 2001

The underpotential deposition (UPD) of Sb on Cu(111), Cu(100) and Cu(110) has been studied using ultra-high vacuum electrochemistry (UHV-EC) techniques. Sb was deposited from acidic chloride solutions and analyzed with Auger electron spectroscopy, low-energy electron diffraction and cyclic voltammetry. A feature observed only in the first voltammetric cycle, starting from the rest potential, appears to be Sb UPD on the copper surfaces. Prior to Sb UPD, Cl structures were observed on each of the three Cu planes. When the potential was scanned into the transient reductive feature, antimony began to deposit, displacing the chlorine. Initially, structures containing both Cl and Sb were formed on the Cu surfaces, including a $(\sqrt{3} \times \sqrt{3})R30^\circ$ on the Cu(111), a $(2\sqrt{2} \times \sqrt{2})R45^\circ$ on the Cu(100), and a structure denoted in matrix notation as $(-\frac{1}{2} \frac{3}{2})$ formed on Cu(110). Further Sb deposition results in displacement of the chloride and new structures on each face: Cu(111)($3 \times \sqrt{21}$)-Sb, Cu(110)(3×2) and Cu(100)(3×2). Scanning the deposition potential further negative, into bulk Sb deposition, yielded no well-ordered structures.

Introduction

Antimony is an increasingly important element in the fields of electronics and optoelectronics. Compound semiconductors containing Sb are used in the formation of infrared (IR) photodetectors, lasers, thermophotovoltaic devices and high-speed electronic devices. Its use as a surfactant and dopant is increasingly important as well.

The III–V compound semiconductors GaSb and InSb are finding an increasing number of applications in the manufacturing of long wavelength (> 1.5 mm) detectors, IR detectors, and high-speed electronics.^{1,2} Other compound semiconductors containing more than two elements, such as $\text{Ga}_x\text{In}_{1-x}\text{As}_y\text{Sb}_{1-y}$ and $\text{InAs}_x\text{Sb}_{1-x}$, can be used for optoelectronic and transport devices.^{3–5}

The second area of semiconductor technology that antimony has shown significance is in alloyed semiconductors. This field involves the formation of alloys of group V and other elements to form semiconducting compounds. Examples of these compounds include Sb_2Te_3 , Sb_2Se_3 , As–Sb alloys and Cs_xSb .^{6–10} Uses for compounds in this area include photocathodes, photodetectors and thermoelectric devices.

An area of high interest for many years has been the use of antimony as a capping layer on III–V compound semiconductors. This capping layer can act as a passivating layer to prevent oxidation or other processes from occurring, or an intermediate layer for the growth of a new compound. These capping layers can also provide information on the growth mechanisms of compound semiconductors. Extensive research has been performed depositing antimony on GaAs.^{11–18} Antimony forms chain-like dimers along the GaAs(110) surface.¹⁷ This is similar to the effect of Bi on GaAs(110) substrates.¹¹ These structures are referred to as epitaxial continued layer structures (ECLS). The chains of the ECLS follow the substrate structure, consisting of antimony atoms lying in troughs of the (110) surface.¹¹ Dimer formation is also evident for the deposition of antimony on GaAs(100), but is less prominent than on the (110) surface.¹⁴ For the GaAs(111) surface, antimony deposition creates a surface reconstruction on the sub-

strate. Various reconstructions, such as (1×3) and (3×8) , can occur depending upon the amount of antimony deposited.^{13,15} Other semiconductor/antimony interfaces that have been studied include InAs, ZnSe, GaP, InP and InAlSb.^{19–24}

Antimony deposition on intrinsic semiconductors, like germanium and silicon, has been studied for analogous reasons to those for its growth on compound semiconductors.^{25–29} The majority of the research in this area has been centered around antimony deposition on silicon. These experiments are designed to probe the surfactant effect of antimony on the growth of metals, given the quasi-metallic nature of Sb. The desire is to form metallic films of metals such as Ag on Si, for example.

Doping of group II–VI compound semiconductors can be accomplished by the incorporation of antimony into the bulk lattice. Cadmium telluride electrodeposited from non-aqueous solutions can be doped with antimony.³⁰ This creates p-type CdTe with few oxygen impurities, due to the oxygen arresting characteristic of antimony. Other semiconductor materials, like SnO_2 , can be doped by antimony incorporation as well.³¹

An interesting area of research concerning antimony deposition is in the surfactant field. Antimony has shown a surfactant effect for the deposition of various metals on a number of substrates.^{26,32–36} The majority of the literature work involves silver deposition, usually on a silver substrate. It is thought that the antimony poisons the silver surface, causing the mobility of the silver adatoms to decrease. This forces the silver atoms to form islands on the substrate, that then coalesce into an epitaxial film.³³

The study presented here involves the deposition of antimony on the low-index planes of copper. While this system has not been studied electrochemically, many surface segregation experiments have been reported.^{37–44} An antimony doped copper single crystal has been used to study the surface structure of this submonolayer coverage of antimony. Scanning tunneling microscopy (STM) and UHV surface analysis have shown that a $(\sqrt{3} \times \sqrt{3})R30^\circ$ antimony/copper surface alloy forms on the Cu(111) surface.^{37,39,40} This alloy consists of antimony atoms sitting in a copper lattice at nominal $\sqrt{3}$

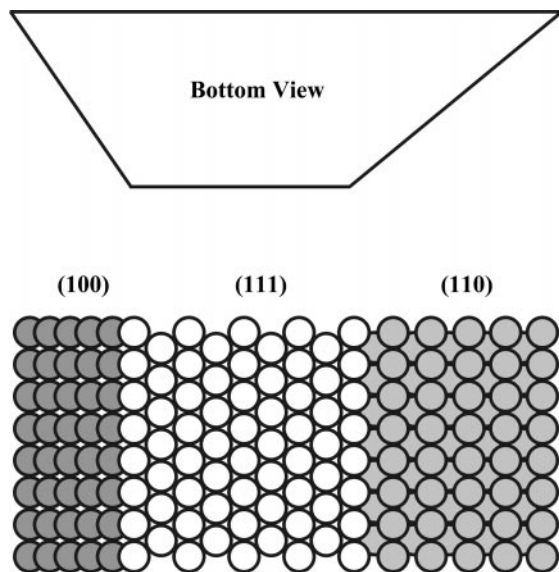


Fig. 1 Cartoon of the copper tri-crystal.

positions. This alloy has been confirmed by medium energy ion scattering (MEIS) techniques.⁴⁴ Several structures arise from the antimony/copper (100) system, depending upon the temperature at which the antimony alloyed copper single crystal is annealed. These structures include $(7\sqrt{2} \times \sqrt{2})R45^\circ$, (2×2) and $(\sqrt{5} \times \sqrt{5})R26^\circ$ unit cells. It appears that the structures are actually alloys, as opposed to adsorbed adlayers.⁴¹

The underpotential deposition (UPD) of antimony could provide a viable technique for the electrochemical deposition of antimony containing compound semiconductors. The underpotential deposition phenomenon involves the electrochemical deposition of a surface limited layer of an element onto a substrate. With certain systems, this first atomic layer is energetically more stable than multiple layers of the element. This UPD layer deposits at a potential prior to that needed to deposit the bulk element. If the potential is held at the UPD value, an atomic layer can deposit at equilibrium, without the formation of bulk, as the reaction is self-terminating. If two elements can be deposited by separate UPD processes, an epitaxial compound can be formed using a cycle. This process is the electrochemical analog of atomic layer epitaxy (ALE), referred to here as electrochemical atomic layer epitaxy (EC-ALE).^{45,46} EC-ALE has been used to form a variety of compound semiconductors.⁴⁷⁻⁴⁹ Progress in the formation of compounds and materials using EC-ALE is

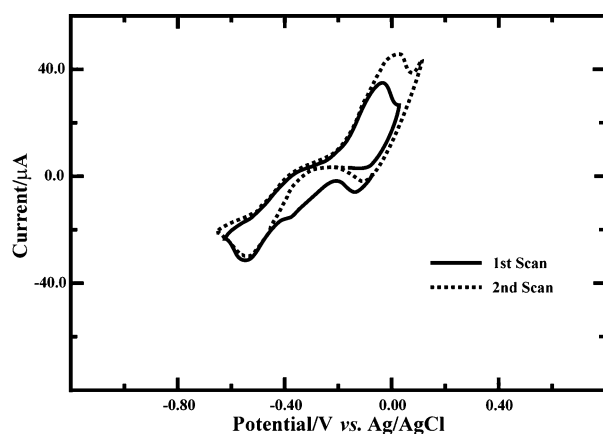


Fig. 2 Cyclic voltammogram of the Cu electrode in 0.1 mM Sb in 1 mM HCl (pH = 3) supporting electrolyte: scan rate = 5 mV s^{-1} .

directly dependent on understanding the atomic layer formation steps needed to form the deposition cycle. Recently, deposits of InSb have been formed using EC-ALE, and the cycle has been incorporated into the formation of InAs/InSb superlattices.⁵⁰ Other compound semiconductors that have been formed by EC-ALE include: CdTe, CdS and CdSe.⁵¹⁻⁵⁷

Experimental

Studies were conducted with a Cu single crystal that had been cut and polished, forming facets of the three low-index planes, (111), (100) and (110), present on one single crystal (Fig. 1).⁵⁸ The three faces are oriented along the vertical axis of the crystal, allowing all three planes to be analyzed in sequence by simply rotating the crystal. The major benefit is that it provides a direct comparison of the structures formed on the Cu low-index planes, formed under a given potential program.

The studies presented here were performed using ultra-high vacuum electrochemical methodologies (UHV-EC),⁵⁹ where the principle is to use a UHV surface analysis instrument, directly coupled to a stainless steel antechamber that houses an electrochemical cell apparatus. This antechamber can be isolated from the main surface analysis chamber and back-filled with ultra-high purity argon before each electrochemical experiment. This allows the direct transfer of the electro-deposited material to the UHV surface analysis chamber, avoiding contamination from air.

This UHV instrument was equipped with a cylindrical mirror analyzer (CMA) for Auger electron spectroscopy (AES) (Physical Electronics), optics for low energy electron diffraction (LEED) (Princeton Electronics), a quadrupole mass analyzer for residual gas analysis (UTI), and an ion gun for cleaning the crystal by ion bombardment (Physical Electronics). The chamber was ion pumped, and a cryo-pump was used to evacuate the antechamber. This cryo-pump was selected due to its high pumping speed of water vapor. The base pressure of the system was usually in the 10^{-9} Torr range, but consisted mostly of Ar and water vapor, which did not interfere with our studies.

Before each electrochemical experiment, the Cu single crystal was cleaned by Ar ion bombardment, followed by annealing to repair damage to the crystal surface. The cleanliness was confirmed by AES and observation of clean surface LEED patterns.

Potentials were measured *vs.* a Ag/AgCl (3 M NaCl) reference electrode (BAS), and the auxiliary electrode was a gold wire (Wilkinson Company). The potentiostat, based on simple op-amp circuitry, was constructed in-house, and was used for voltammetry and the control of electrode potentials. The Sb solution consisted of 0.1 mM Sb (Sb_2O_3 , 99.999% Aldrich), and 1 mM HCl (reagent grade, J. T. Baker). An acidic solution was used not only to facilitate the dissolution of the Sb_2O_3 , but also to prevent the formation of CuO_x species during experiments. Ultra-pure (18 M Ω) water from a nanopure filtration system (Barnstead), fed from the house-deionized water supply, was used to prepare the antimony solution.

The electrochemical hardware consisted of a Pyrex H-cell housed in a stainless steel cylinder. This allowed the cell to be purged with ultra-pure Ar prior to each electrochemical experiment. The cell was introduced into the EC-antechamber, which was backfilled to atmospheric pressure with ultra-pure Ar, through a gate valve at the bottom. Solutions were pumped into the H-cell by pressurizing the Pyrex solution reservoirs. Each bottle was equipped with a glass-tee with a three-way stopcock, allowing solution delivery and its subsequent draining.

After Sb deposition, the solutions were drained, the electrochemical cell was withdrawn, the gate valve closed, and the EC-antechamber was evacuated using cryosorption pumps and the cryo-pump. Upon reaching ultra-high vacuum, the

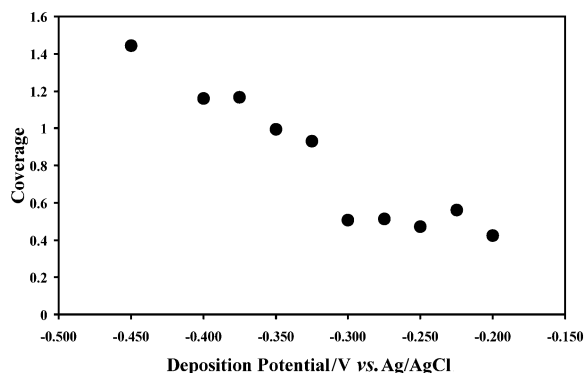


Fig. 3 Coverage calculated by coulometric data *vs.* deposition potential.

crystal was transferred back into the main chamber for surface analysis. AES spectra, with 3000 eV ionizing electrons, were collected for each face of the crystal, for kinetic energies between 100–1100 eV. LEED patterns were recorded for each plane using a Kodak digital camera (Model DC290).

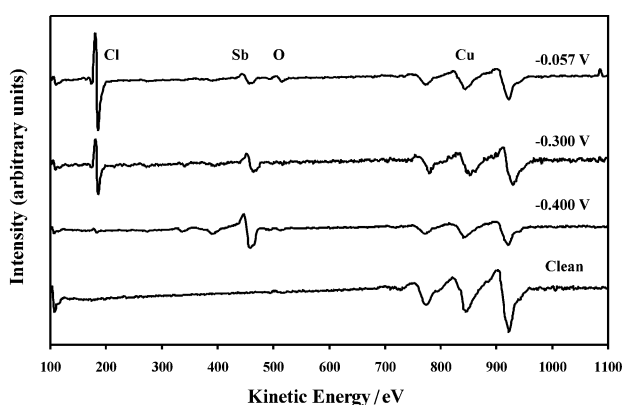


Fig. 4 AES spectra for Sb/Cl deposition of the Cu(111) surface of the copper electrode at various deposition potentials.

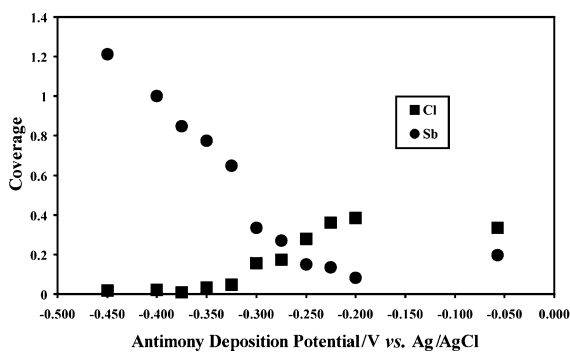


Fig. 5 Coverages calculated from Auger peak ratios *vs.* deposition potential for Cu(111).

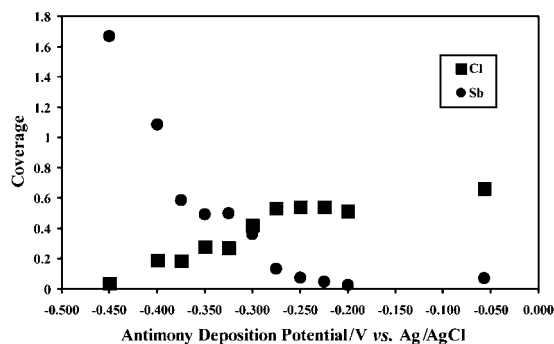


Fig. 6 Coverages calculated from Auger peak ratios *vs.* deposition potential for Cu(100).

Results and discussion

Cyclic voltammetry for the clean, annealed copper tri-crystal in the Sb solution is shown in Fig. 2. The scans were started at the rest potential, -0.057 V, and then scanned between -0.7 V and -0.1 V for two cycles. A scan rate of 5 mV s^{-1} was used.

The first reduction feature, at -0.1 V, is due to a small amount of dissolved copper re-depositing onto the electrode surface. The broad reduction shoulder at -0.4 V appears only in the first scan. This feature was never observed in subsequent scans, regardless of how far positive the oxidation potential was scanned. This reduction is believed to be the underpotential deposition of antimony onto the copper electrode. Oxidation of the UPD antimony does not occur with these conditions, as copper dissolution takes place first, depolarizing the electrode, and preventing the dissolution of the last atomic layer of Sb. The reduction feature at -0.600 V and the oxidation feature at 0.000 V are the deposition and stripping of bulk Sb, respectively.

In the studies presented here, antimony was deposited on the clean copper crystal by immersion in the solution at a series of controlled potentials. Each deposition was performed for 2 min. The resulting coulometric data is shown in Fig. 3, where a short plateau is evident between -0.200 to -0.300 V, suggesting surface limited deposition, consistent with UPD. After this plateau, the coverage increases to near 1.0 and continues to rise, at potentials below -0.400 V. The currents measured in each experiment are the result of not only the deposition of antimony on each low-index plane, but also of the reductive dissolution of an adsorbed monolayer of chlorine. This masks the Sb coverage based coulometry, although the charges provide an estimation of expected coverages.

Auger spectra for each of the three low-index planes were collected after each emersion experiment. At potentials positive of -0.2 V, only chlorine and copper were evident, with very little antimony present (coverages less than 0.15 ML). The small amount that was present appears to have been antimony oxide adsorbed to the surface. This is evident due to the oxygen signal present in the Auger spectra. At potentials more negative than -0.200 V, reduced antimony began to deposit on the electrode, with a corresponding decrease in the chlorine coverage. This decrease in the Cl signal varies between the three faces. On the Cu(111), the chlorine intensity dropped to near zero, but a significant signal was still present for the Cu(100) and Cu(110) throughout the potential range used in these studies.

Fig. 4 shows four typical Auger spectra at various emersion potentials for the Cu(111) surface. Auger peak heights for antimony, chlorine, and copper were measured for each spectrum and used to calculate Auger peak ratios for antimony/copper and chlorine/copper. These ratios were then plotted *vs.* the corresponding deposition potential. The copper peak at 920 eV, the chlorine peak at 181 eV, and the antimony peak at 454 eV were chosen for the Auger peak measurements. Since coulometric data could not be used to accurately predict coverages in these experiments, the Auger peak ratios were converted into coverages. This was accomplished by assuming that at -0.057 V the Cl coverage for the Cu(111) surface is 0.33. This was confirmed by LEED and by the literature.^{60–62} Using this coverage and the corresponding Auger peak ratio, the remaining Auger peak ratios were converted into coverages for each low-index plane. Similarly, the Sb coverage at -0.300 V, from LEED and literature values, was assumed to be 0.33.³⁷ The Sb/Cu Auger peak ratios were then converted into coverages in the same manner as for the Cl/Cu ratios. These coverages were plotted *vs.* the deposition potential for all three low-index planes (Fig. 5–7). These coverages, combined with the LEED data (Fig. 8–10), were used to construct the proposed structures for each face (Fig. 11–13).

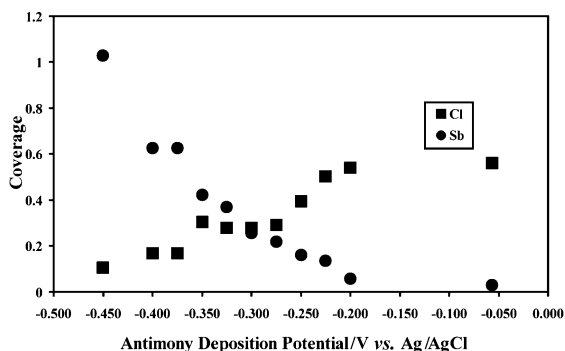


Fig. 7 Coverages calculated from Auger peak ratios *vs.* deposition potential for Cu(110).

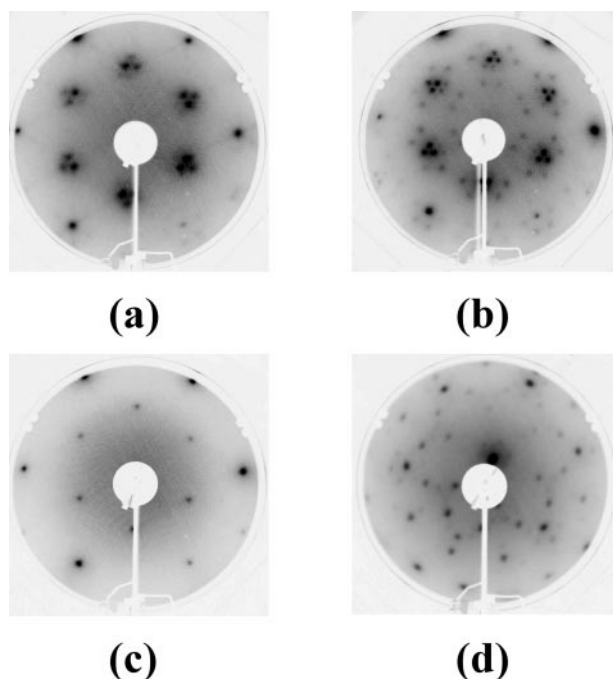


Fig. 8 LEED patterns for the Cu(111) surface. Deposition potential: (a) -0.057 , (b) -0.200 , (c) -0.300 , (d) -0.350 V.

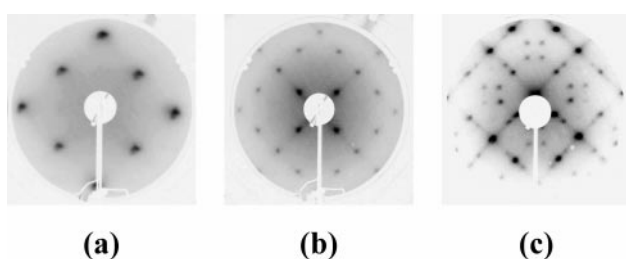


Fig. 9 LEED patterns for the Cu(100) surface. Deposition potential: (a) -0.057 , (b) -0.300 , (c) -0.350 V.

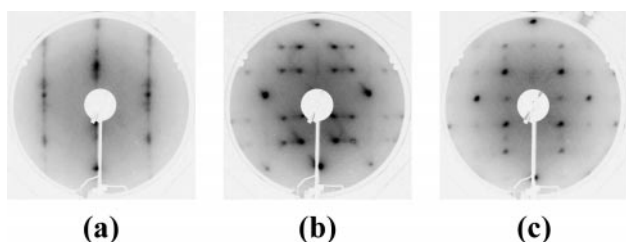


Fig. 10 LEED patterns for the Cu(110) surface. Deposition potential: (a) -0.057 , (b) -0.300 , (c) -0.350 V.

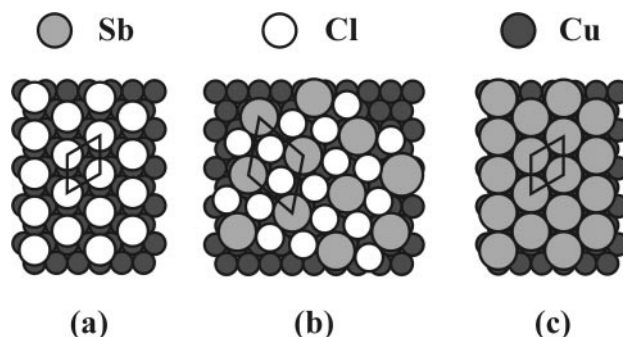


Fig. 11 Proposed structures for the Cu(111) surface adlayers. (a) Cl "split-spot" ($\sqrt{3} \times \sqrt{3}$) $R30^\circ$, (b) Sb/Cl transition ($\sqrt{7} \times \sqrt{7}$) $R19.1^\circ$, (c) Sb ($\sqrt{3} \times \sqrt{3}$) $R30^\circ$.

Chlorine has been shown to deposit spontaneously on Cu surfaces over a wide range of potentials.^{60–65} At potentials positive of -0.200 V, Cl is present on all three Cu planes. A "split-spot" ($\sqrt{3} \times \sqrt{3}$) $R30^\circ$ LEED pattern was observed for the Cu(111) surface (Fig. 8(a)). This "split-spot" pattern has a group of spots, three to six, near the LEED pattern's $\sqrt{3}$ positions. The splitting of the spots has been explained elsewhere either by $\sqrt{3}$ local symmetry inside a larger unit cell with phase boundaries or by a ($p \times \sqrt{3}$) structure as seen by STM studies.^{60,63,66} This has been observed for other systems, such as iodine adsorption on Cu and silver, and tellurium adsorption on gold.^{48,67–69} It is also observed that the "split-spot" pattern is only observed *ex-situ* and not while imaged in solution with a scanning tunneling microscope.⁷⁰ Since the LEED experiments were conducted *ex-situ*, the proposed structure derived is the split-spot ($\sqrt{3} \times \sqrt{3}$) $R30^\circ$ (Fig. 11(a)).

On the Cu(100) surface, a ($\sqrt{2} \times \sqrt{2}$) $R45^\circ$ structure is formed by the Cl adlayer (Fig. 9(a)). This structure is equiva-

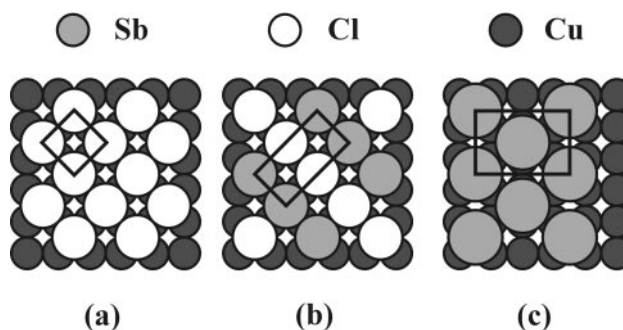


Fig. 12 Proposed structures for the Cu(100) surface adlayers. (a) Cl ($\sqrt{2} \times \sqrt{2}$) $R45^\circ$, (b) Sb/Cl ($2\sqrt{2} \times 2\sqrt{2}$) $R45^\circ$, (c) Sb (3×2).

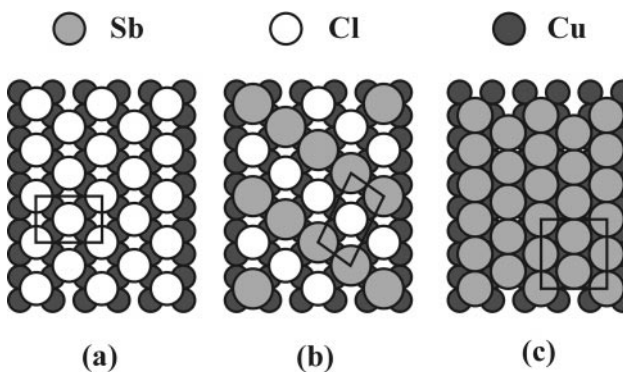


Fig. 13 Proposed structures for the Cu(110) surface adlayers. (a) Cl $c(2 \times 2)$, (b) Sb/Cl matrix denoted, (c) Sb (3×2).

Table 1 Chlorine structures and coverages: ideal and experimental

Face	Surface atoms/cm ⁻²	Cl structure	Ideal Cl atoms cm ⁻²	Normalized Auger pp ratio Cl/Cu ₂ atoms cm ⁻²
(111)	1.76 × 10 ¹⁵	(√3 × √3)R30°	5.9 × 10 ¹⁴	5.87 × 10 ¹⁴
(100)	1.52 × 10 ¹⁵	(√2 × √2)R45°	7.6 × 10 ¹⁴	7.69 × 10 ¹⁴
(110)	1.08 × 10 ¹⁵	c(2 × 2)	5.4 × 10 ¹⁴	5.57 × 10 ¹⁴

lent to the c(2 × 2) structure seen in gas-phase Cl dosing studies of Cu(100).⁶⁰ The coverage *vs.* deposition potential plot indicates a coverage of 0.5, which agrees well with previous work, and the symmetry of the LEED pattern. The proposed structure for this Cl adlayer is shown in Fig. 12(a).

The LEED pattern for the Cu(110) surface coated with Cl is streaky, consisting of a series of broad lines (Fig. 10(a)). This pattern is representative of a c(2 × 2) structure. The explanation for this diffuse pattern is that there are multiple unit cells simultaneously distributed across the (110) surface.⁶⁰ This structure is probably due to chains of Cl atoms in the troughs of the corrugated Cu surface. These atoms are free to move along the troughs, producing a variety of unit cells and thus the streaks in the LEED pattern. A simple c(2 × 2) structure yields a coverage value equal to 0.5 (Fig. 13(a)). The coverage for this proposed structure is consistent with the Auger data (Fig. 7).

At approximately -0.200 V, a (√7 × √7)R19.1° pattern begins to mix into the “split-spot” Cl pattern for the Cu(111) (Fig. 8(b)). Auger data shows an increased Sb signal for this deposition potential, and the intensity of the Cl peaks begins to decrease. The √7 spots that appear in the LEED pattern are believed to be due to the incorporation of Sb into the adlayer of Cl. The proposed structure at this potential has Cl maintaining its (√3 × √3)R30° lattice, while the Sb is beginning to form structural domains with (√7 × √7)R19.1° symmetry, displacing some of the Cl (Fig. 11(b)). Coverages for both the Sb and the Cl agree between the proposed structure and the Auger peak ratios. Alternatively, the Sb may just insert into the (√3 × √3)R30° lattice, creating a larger unit cell that contains both Sb and Cl atoms. Another possibility is that two different domains form once the Sb begins to deposit, one being the (√3 × √3)R30° Cl and the other being the (√7 × √7)R19.1° Sb. This would be a good system for study using scanning tunneling microscopy.

The Cu(100) surface shows no change at -0.200 V from its original (√2 × √2)R45° coverage. Auger spectroscopy does show a small Sb signal at this potential, but the LEED pattern is unchanged. LEED patterns for the Cu(110) face at -0.200 V show no discernible pattern. Many highly diffuse spots are present in these patterns, but no clear structure is visible. This pattern is thought to be a transition from the c(2 × 2) to a different pattern containing both Cl and Sb, due to the increase in the Sb Auger signal.

At an emersion potential of -0.300 V, a sharp (√3 × √3)R30° LEED pattern is present for the Cu(111) surface (Fig. 8(c)). No splitting of the LEED spots is observed. This pattern is consistent with scanning tunneling microscopy

data for the surface segregation of Sb on Cu(111).^{37,39} Aufray and co-workers discovered evidence of an Sb/Cu alloy phase in their STM studies. The Sb occupied positions equivalent to a (√3 × √3)R30° adlayer, but the atoms were actually bound into the first layer of the Cu substrate. This phenomenon can neither be proved nor disproved by the data presented here. While the Cl Auger signal has diminished substantially, a significant amount of Cl is still present upon the surface. It is not known if this Cl is incorporated into the proposed (√3 × √3)R30° structure (Fig. 11(c)).

The Cl/Cu and Sb/Cu Auger peak ratios are nearly equal for the Cu(110) face at -0.300 V. LEED displays a well-defined pattern (Fig. 10(b)) at this potential, apparently related to the (2√2 × √2)R45° structure formed on Cu(100). This pattern is described using matrix notation as: $\begin{pmatrix} -1 & 3 \\ 1 & 1 \end{pmatrix}$. From the coverage *vs.* potential graphs, the structure should be composed of 0.25 coverages for both Sb and Cl. The unit cell, derived from the LEED, is consistent with these coverages as well, implying the Cl and the Sb may form overlapping structures with the same unit cell (Fig. 13(b)).

For the Cu(100), a new structure is also observed at -0.300 V. The LEED pattern is a (2√2 × √2)R45° for the Sb/Cl layer (Fig. 9(b)). The Cl signal in the Auger spectrum is decreased, but is still prominent. Coverages for both the Sb and Cl are both approximately 0.4 (Fig. 6), slightly higher than the 0.25 coverages in the proposed structure for this potential (Fig. 12(b)).

At a deposition potential of -0.350 V, a (3 × 2) LEED pattern is observed for the deposited Sb on Cu(100) (Fig. 9(c)). The Sb coverage calculated from the Auger peak ratios is approximately 0.5, while the Cl is 0.25 (Fig. 6). The proposed structure is a simple (3 × 2) unit cell with an extra Sb atom centered in the cell (Fig. 12(c)). This gives a coverage of only 0.33 for the Sb. While this is slightly lower than the Auger coverage, it was the only logical structure devised that was consistent with the unit cell. The explanation for the discrepancy between the LEED and Auger peak ratios is not known.

At -0.350 V, the Cu(111)(√3 × √3)R30°-Sb structure changes to a (3 × √21) unit cell (Fig. 8(d)). According to Auger data, the Sb coverage is approximately 0.75. No logical structure has been devised as yet to account for this coverage and the (3 × √21) unit cell. One possibility for this unusual coverage is alloy formation. It has been reported through segregation experiments that Sb will alloy into the first layer of the Cu single crystal.^{37,39,40} This forms an SbCu₂ alloy layer, with the Sb atoms sitting within √3 sites in the lattice as discussed above. If a second layer of pure antimony deposits upon this alloy, the (3 × √21) unit cell may be formed giving

Table 2 Antimony structures and coverages: ideal and experimental

Face	Surface atoms cm ⁻²	Sb structure	Ideal Sb atoms cm ⁻²	Normalized Auger pp ratio Sb/Cu ₂ atoms cm ⁻²
(111)	1.76 × 10 ¹⁵	(√3 × √3)R30°	5.9 × 10 ¹⁴	5.87 × 10 ¹⁴
(100)	1.52 × 10 ¹⁵	(2√2 × √2)R45°	7.6 × 10 ¹⁴	3.90 × 10 ¹⁴
(110)	1.08 × 10 ¹⁵	Matrix denoted	5.4 × 10 ¹⁴	3.91 × 10 ¹⁴
(111)	1.76 × 10 ¹⁵	(3 × √21)	5.9 × 10 ¹⁴	1.36 × 10 ¹⁵
(100)	1.52 × 10 ¹⁵	(3 × 2)	7.6 × 10 ¹⁴	5.33 × 10 ¹⁴
(110)	1.08 × 10 ¹⁵	(3 × 2)	7.2 × 10 ¹⁴	6.48 × 10 ¹⁴

a total Sb coverage of near 0.75. It is assumed that the Sb arranges in a hexagonal overlayer, but the exact structure cannot be determined from LEED and AES alone. Further STM studies are needed to fully understand this coverage.

The 0.25 coverage ($\begin{smallmatrix} -1 & 3 \\ 1 & 1 \end{smallmatrix}$) unit cell for the Cu(110) changes to a more densely packed adlayer at -0.400 V. This new structure gives a (3×2) LEED pattern (Fig. 10(c)). The Auger plots suggest an Sb coverage of approximately 0.66 at this potential. This yields a proposed structure that is identical to the high-density coverage for Cl adsorbed on Cu(110) (Fig. 13(c)).⁶⁰ The Cl coverage is diminished, but still present. Again, it is not known where this Cl resides in this structure.

Beyond -0.450 V, no discernible LEED patterns are visible for the three low-index planes. It is assumed that beyond this potential the Sb deposition is mass transfer controlled, not UPD. Coverages for the Sb in this range exceed 1.0 and the Cl coverages are reduced to nearly zero.

Table 1 shows the ideal and experimental coverages for the Cl structures. Good correlation exists between the theoretical and measured values. These results also agree closely with previous work on the exposure of Cu single crystals to gaseous Cl_2 and aqueous Cl^- solutions.^{60,64}

Ideal and experimental coverages for the Sb structures are tabulated in Table 2. Correlations between the ideal and experimental values vary for each surface. For Cu(111), the 0.33 coverage ($\sqrt{3} \times \sqrt{3}$) $R30^\circ$ structure, experimental and ideal values have to match due to the assumption made in calculating the theoretical coverages. The $(3 \times \sqrt{21})$ structure gives a coverage that is nearly twice the ideal 0.33 coverage, clearly illuminating the fact that the unit cell basis is not well understood.

Both the $(2\sqrt{2} \times \sqrt{2})R45^\circ$ on Cu(100) and the matrix denoted structure on Cu(110) show lower experimental coverages when compared to the ideal structures. This is probably related to the finite amount of Cl adsorbed on the surface. The presence of Cl on the surface may in some way limit the Sb coverage, relative to the ideal value. This also appears to happen in the (3×2) structures on both Cu(100) and Cu(110). It is proposed that the Cl has the same unit cell as the Sb for the $(2\sqrt{2} \times \sqrt{2})R45^\circ$ and matrix denoted structures. The actual placement of the Cl on the two (3×2) structures is not known and is clearly an area where STM studies are needed.

Conclusions

Antimony atomic layers have been electrodeposited from acidic chloride solutions onto the low-index planes of Cu by UPD. Cl initially deposits as well-ordered structures on the Cu single crystal forming a $(\sqrt{3} \times \sqrt{3})R30^\circ$ on Cu(111), a $(\sqrt{2} \times \sqrt{2})R45^\circ$ on Cu(100) and a $c(2 \times 2)$ on Cu(110). Those structures are present until the onset of Sb deposition. Each plane of the Cu single crystal forms a transition structure composed of both Sb and Cl, beginning at about -0.200 V.

As the potential is scanned to more negative values, the Sb coverage increases and the Cl coverage decreases. On the Cu(111) surface, the Sb adlayer forms a $(\sqrt{3} \times \sqrt{3})R30^\circ$ structure with a small amount of Cl still present. This structure is present until the onset of a $(3 \times \sqrt{21})$ unit cell at -0.350 V. At this point, the Cl coverage is nearly zero and the Sb coverage is approximately 0.75. The basis for this unit cell is not known, and STM data is needed.

The Cu(100) $(2\sqrt{2} \times \sqrt{2})R45^\circ$ transition structure changes into a (3×2) unit cell at -0.350 V. This structure gives a Sb coverage of 0.5, while the Cl is at 0.25. The ideal coverage for this unit cell is 0.33. The reason for the discrepancy between these values is unknown.

The matrix denoted structure for the Sb adlayer on Cu(110) transforms into a (3×2) structure upon further Sb deposition at -0.400 V. The calculated coverage and experimental coverage values are approximately equal at 0.67. A small amount of

Cl, about 0.2 ML, is still present on the surface, but it is not known how this Cl affects the structure. Beyond -0.450 V, no well-ordered structures were observed, and the Sb coverages increase above 1 ML.

These results demonstrate that a surface-limited reaction does occur in the electrodeposition of Sb onto the low-index planes of Cu. A sequence of ordered structures was observed on each of the low-index planes. It is clear that the structures are very dependent on the electrolyte, in this case Cl^- . A well-defined UPD process does take place, even though it is not present in the voltammetry.

Acknowledgements

Support from the National Science Foundation, Division of Materials Research, is gratefully appreciated, as well as support from the University of Georgia Research Foundation.

References

- 1 N. Jones, C. Norris, C. L. Nicklin, P. Steadman, S. H. Baker, A. D. Johnson and S. L. Bennett, *Surf. Sci.*, 1998, **409**, 27.
- 2 I. Nicoara, D. Nicoara, A. G. Ostrogorsky, C. Marin and T. Peignier, *J. Cryst. Growth*, 2000, **220**, 1.
- 3 H. Baaziz, Z. Charifi and N. Bouarissa, *Mater. Chem. Phys.*, 2001, **68**, 197.
- 4 S. Cattarin, M. M. Musiani, U. Casellato, P. Guerriero and R. Bertinello, *J. Electroanal. Chem.*, 1995, **380**, 209.
- 5 J. J. Lee and M. Razeghi, *J. Cryst. Growth*, 2000, **221**, 444.
- 6 B. Erjavec, *Thin Solid Films*, 1997, **303**, 4.
- 7 A. M. Fernandez and M. G. Merino, *Thin Solid Films*, 2000, **366**, 202.
- 8 M. M. Musiani, F. Paolucci and P. Guerriero, *J. Electroanal. Chem.*, 1992, **332**, 113.
- 9 M. Monev, I. Krastev and A. Zielonka, *J. Phys.-Condens. Matter*, 1999, **11**, 10033.
- 10 R. Venkatasubramanian, T. Colpitts, E. Watko, M. Lamvik and N. El-Masry, *J. Cryst. Growth*, 1997, **170**, 817.
- 11 P. Haier, P. V. Santos, N. Esser and W. Richter, *Surf. Sci.*, 1998, **399**, 264.
- 12 P. V. Santos, N. Esser, J. Groenen, M. Cardona, W. G. Schmidt and F. Bechstedt, *Phys. Rev. B*, 1995, **52**, 17379.
- 13 P. Moriarty, P. H. Beton, M. Henini and D. A. Woolf, *Surf. Sci.*, 1996, **365**, L663.
- 14 F. Maeda, Y. Watanabe and M. Oshima, *Surf. Sci.*, 1996, **357–358**, 540.
- 15 A. A. Cafolla, C. McGinley, E. McLoughlin, G. Hughes, P. Moriarty, A. W. Dunn, Y. R. Ma, D. Teehan, B. Murphy, S. Downes and D. A. Woolf, *Surf. Sci.*, 1997, **377–379**, 130.
- 16 W. G. Schmidt and F. Bechstedt, *Surf. Sci.*, 1997, **377–379**, 11.
- 17 C. Nowak, A. Hempelmann, A. Markl, A. Chasse, E. Dudzik, C. Muller, I. T. McGovern, W. Braun, W. Richter and D. R. T. Zahn, *Surf. Sci.*, 1995, **331–333**, 564.
- 18 L. J. Whitman, B. R. Bennett, E. M. Kneedler, B. T. Jonker and B. V. Shanabrook, *Surf. Sci.*, 1999, **436**, L707.
- 19 V. Y. Aristov, M. Grekh, V. M. Zhilin, A. Taleb-Ibrahimi, G. Indlekofer, Z. Hurych, G. Le Lay and P. Soukiassian, *Appl. Surf. Sci.*, 1996, **104/105**, 73.
- 20 S. A. Clark, J. W. Cairns, S. P. Wilks, R. H. Williams, A. D. Johnson and C. R. Whitehouse, *Surf. Sci.*, 1995, **336**, 193.
- 21 D. Drews, A. Schneider, D. R. T. Zahn, D. Wolfram and D. A. Evans, *Appl. Surf. Sci.*, 1996, **104/105**, 485.
- 22 M. G. Betti, V. Martinelli and C. Mariani, *Phys. Rev. B*, 1998, **57**, 4544.
- 23 W. K. Ford, T. Guo, K. J. Wan and C. B. Duke, *Phys. Rev. B*, 1992, **45**, 11896.
- 24 C. Nowak, J. Krujatz, A. Markl, C. Meyne, A. Chasse, W. Braun, W. Richter and D. R. T. Zahn, *Surf. Sci.*, 1995, **331–333**, 619.
- 25 S. Nakatani, Y. Kuwahara, T. Takahashi and M. Aono, *Surf. Sci.*, 1996, **357–358**, 65.
- 26 K. H. Park, J. S. Ha, S. J. Park and E. H. Lee, *Surf. Sci.*, 1997, **380**, 258.
- 27 A. A. Saranin, A. V. Zotov, V. G. Lifshits, O. Kubo, T. Harada, M. Katayama and K. Oura, *Surf. Sci.*, 2000, **447**, 15.
- 28 M. Ladeveze, G. Treglia, P. Muller and F. Arnaud d'Avitaya, *Surf. Sci.*, 1998, **395**, 317.
- 29 G. Falkenberg, L. Seehofer and R. L. Johnson, *Surf. Sci.*, 1997, **377–379**, 75.

- 30 J. P. Nair, R. Jayakrishnan, N. B. Chaure, A. Lobo, S. K. Kulkarni and R. K. Pandey, *Thin Solid Films*, 1999, **347**, 39.
- 31 K. Y. Rajpure, M. N. Kusumade, M. N. Neumann-Spallart and C. H. Bhosale, *Mater. Chem. Phys.*, 2000, **64**, 184.
- 32 M. Jiang, M. Qiu, Y. J. Zhao and P. L. Cao, *Phys. Lett. A*, 1998, **239**, 127.
- 33 M. Jiang, X. Y. Zhou, M. Qiu and P. L. Cao, *J. Phys.-Condens. Matter*, 1998, **10**, 8653.
- 34 M. Jiang, Y. J. Zhao and P. L. Cao, *Phys. Rev. B*, 1998, **57**, 10054.
- 35 S. Oppo, V. Fiorentini and M. Scheffler, *Phys. Rev. Lett.*, 1993, **71**, 2437.
- 36 B. Voigtlander and A. Zinner, *Surf. Sci.*, 1996, **351**, L233.
- 37 B. Aufray, H. Giordano and D. N. Seidman, *Surf. Sci.*, 2000, **447**, 180.
- 38 I. Meunier, J. M. Gay, L. Lapena, B. Aufray, H. Oughaddou, E. Landemark, G. Falkenberg, L. Lottermoser and R. L. Johnson, *Surf. Sci.*, 1999, **422**, 42.
- 39 M. Gothelid, B. Aufray, H. Giordano, J. M. Gay, G. Le Lay, R. Belkhou, N. Marsot and C. Guillot, *Surf. Rev. Lett.*, 1997, **4**, 1203.
- 40 H. Giordano and B. Aufray, *Surf. Sci.*, 1996, **352**, 280.
- 41 H. Giordano, J. P. Biberian and B. Aufray, *Surf. Sci.*, 1994, **313**, 266.
- 42 H. Giordano and B. Aufray, *Surf. Sci.*, 1994, **309**, 816.
- 43 H. Giordano, O. Alem and B. Aufray, *Scrip. Metall. Mater.*, 1993, **28**, 257.
- 44 P. Bailey, T. C. Q. Noakes and D. P. Woodruff, *Surf. Sci.*, 1999, **426**, 358.
- 45 B. W. Gregory and J. L. Stickney, *J. Electroanal. Chem.*, 1991, **300**, 543.
- 46 B. W. Gregory, D. W. Suggs and J. L. Stickney, *J. Electrochem. Soc.*, 1991, **138**, 1279.
- 47 A. Gichuhi, B. E. Boone and C. Shannon, *Langmuir*, 1999, **15**, 763.
- 48 T. A. Sorenson, K. Varazo, D. W. Suggs and J. L. Stickney, *Surf. Sci.*, 2001, **470**, 197.
- 49 J. L. Stickney, in *Electroanalytical Chemistry A Series of Advances*, ed. A. J. Bard and I. Rubinstein, Marcel Dekker, New York, 1999, p. 75.
- 50 T. L. Wade, R. Vaidyanathan, U. Happek and J. L. Stickney, *J. Electroanal. Chem.*, 2001, **500**, 322.
- 51 L. P. Colletti, B. H. Flowers, Jr. and J. L. Stickney, *J. Electrochem. Soc.*, 1998, **145**, 1442.
- 52 L. P. Colletti and J. L. Stickney, *J. Electrochem. Soc.*, 1998, **145**, 3594.
- 53 L. P. Colletti, D. Teklay and J. L. Stickney, *J. Electroanal. Chem.*, 1994, **369**, 145.
- 54 T. E. Lister, L. P. Colletti and J. L. Stickney, *Isr. J. Chem.*, 1997, **37**, 287.
- 55 D. W. Suggs and J. L. Stickney, *Surf. Sci.*, 1993, **290**, 362.
- 56 D. W. Suggs and J. L. Stickney, *Surf. Sci.*, 1993, **290**, 375.
- 57 B. M. Huang, L. P. Colletti, B. W. Gregory, J. L. Anderson and J. L. Stickney, *J. Electrochem. Soc.*, 1995, **142**, 3007.
- 58 J. L. Stickney, C. B. Ehlers and B. W. Gregory, in *Electrochemical Surface Science*, ed. M. P. Soriaga, ACS Press, Washington, 1988, p. 99.
- 59 M. P. Soriaga and J. L. Stickney, in *Modern Techniques in Electroanalysis*, ed. P. Vanysek, John Wiley & Sons, New York, 1996, p. 1.
- 60 J. L. Stickney, C. B. Ehlers and B. W. Gregory, *Langmuir*, 1988, **4**, 1368.
- 61 T. P. Moffat, in *Electrochemical Processing in ULSI Fabrication and Semiconductor/Metal Deposition II*, ed. P. C. Andricacos, P. C. Searson, C. Reidsema-Simpson, P. Allongue, J. L. Stickney and G. M. Oleszek, The Electrochemical Society, Pennington, NJ, 1999, p. 41.
- 62 J. Inukai, Y. Osawa and K. Itaya, *J. Phys. Chem. B*, 1998, **102**, 10034.
- 63 L. J. Wan and K. Itaya, *J. Electroanal. Chem.*, 1999, **473**, 10.
- 64 J. L. Stickney, B. W. Gregory and C. Ehlers, *J. Electrochem. Soc.*, 1988, **135**, C158.
- 65 T. P. Moffat, in *Electrochemical Synthesis and Modification of Materials*, ed. P. C. Andricacos, S. G. Corcoran, J. L. Delplancke, T. P. Moffat and P. C. Searson, Materials Research Society, Pittsburgh, PA, 1997, p. 75.
- 66 B. V. Andryushechkin, K. N. Eltsov and V. M. Shevlyuga, *Surf. Sci.*, 2000, **470**, L63.
- 67 B. V. Andryushechkin, K. N. Eltsov and V. M. Shevlyuga, *Surf. Sci.*, 2001, **472**, 80.
- 68 S. B. Diczko, G. K. Wertheim and D. N. E. Buchanan, *Surf. Sci.*, 1982, **121**, 411.
- 69 G. N. Salaita, F. Lu, L. Lagurendavidson and A. T. Hubbard, *J. Electroanal. Chem.*, 1987, **229**, 1.
- 70 P. Broekmann, M. Wilms, M. Kruff, C. Stuhlmann and K. Wandelt, *J. Electroanal. Chem.*, 1999, **467**, 307.